Available online at www.sciencedirect.com
SCIENCE DIRECT®
Journal of Power Sources 138 (2004) 174–186
JOURNAL OF POWER SOURCES
www.elsevier.com/locate/jpowsour

A macro-level model for determining the performance characteristics of solid oxide fuel cells

Eduardo Hernández-Pacheco[a,*], Devinder Singh[a], Phillip N. Hutton[b], Nikhil Patel[b], Michael D. Mann[a]

[a] *Department of Chemical Engineering, University of North Dakota, Grand Forks, ND 58202, USA*
[b] *Energy & Environmental Research Center, University of North Dakota, Grand Forks, ND 58202, USA*

Received 16 June 2004; accepted 29 June 2004
Available online 21 August 2004

Abstract

This work presents a macro-level model to determine the performance characteristics of solid oxide fuel cells (SOFCs). Activation, ohmic, and concentration polarizations are considered the main sources of irreversibility. The Butler–Volmer equation, the dusty gas model, and Ohm's law were used to determine the polarization terms. Tafel equation, linear current potential, Fick's model, and Stefan–Maxwell model were quantitatively analyzed as well. Performance curves were calculated for hydrogen, methane, and carbon monoxide as pure fuels at different conditions. A surface plot for each polarization term allowed us to analyze the contribution to voltage loss as a function of temperature and current density. The calculations presented in this paper involved the creation of many computational tools. One sample code of these algorithms is included, but all algorithms used in the paper are available from the authors.

Keywords: SOFC; Ohmic; Activation; Concentration; Polarization; Performance fuel cell

1. Introduction

Solid oxide fuel cells (SOFCs) operate at high temperature (800–1200 °C), which makes possible the use of a variety of fuels (hydrocarbons), cogeneration, and bottoming cycles. The Energy & Environmental Research Center (EERC) at the University of North Dakota (UND) designed a thermally integrated biomass SOFC-gasification system (BG-SOFC). The producer gas (a mixture of hydrogen, methane, carbon monoxide, carbon dioxide, small amounts of tars <1%, and steam) from the gasifier will be fed into the SOFC, and the hot effluent gases from the anode and cathode will be reinjected into the gasifier (at different gasification zones), maintaining the reactor temperature. At high temperatures (≈600 °C), methane will be internally reformed in the SOFC and carbon monoxide will be converted to hydrogen (assuming that the water–gas shift reaction will always be at equilibrium) [1,2]. Conversion efficiencies are expected up to 45% based on modeling analyses [3]. The accurate prediction of SOFC operating conditions is important for attaining high efficiencies and successfully integrating both systems (BG-SOFC). The spectrum of possible operating conditions can be determined based on the performance characteristics of the fuel cell. These characteristics will allow us to determine a set of operating conditions (temperature, pressure, inlet compositions) for optimal performance.

The fuel cell performance is subject to the second law of thermodynamics so that losses in the system are inevitable. For a fuel cell, the main source of irreversibility comes from (1) ionic resistance through the electrolyte and electronic resistance on the electrodes and interconnects, (2) activation energy, and (3) the diffusion of gases to the reaction sites. These losses can be determined numerically or experimentally (see [4,5] for experimental-related literature). However, numerical models are preferred for economical reasons and

* Corresponding author. Tel.: +1 7017779495.
E-mail address: ehernand@und.nodak.edu (E. Hernández-Pacheco).

0378-7753/$ – see front matter © 2004 Elsevier B.V. All rights reserved.
doi:10.1016/j.jpowsour.2004.06.051

because sensitivity to different parameters can be investigated with the same model. There are, in general, three types of numerical models used for determining the polarization terms in SOFCs: micro-level models [6–10], macro-level models [11–14], and semiempirical models [15–17]. Results presented in this paper are based on a macro-level model. This model is based on the assumption that the reactions occur at the electrode–electrolyte interface, and therefore no analysis at the microscopic level is required. This assumption is valid for pure electronic conductors but is unrealistic for cermet-type anodes, because of the intermixing in the electrode–electrolyte interface. However, based on the cermet-modeling results by Chan and Xia [18], it can be argued that most of the polarization contribution occurs at the interface, especially for anode-supported cells with thick anodes (≈600 μm). The objective of this paper is to present a set of computational tools for predicting the polarization terms in anode-supported cells using a macro-level model. The model presented here can be extended into a system model that includes temperature and flow distributions, and this work will be presented in the future.

Section 2 describes different approaches to calculate the polarization terms (i.e., activation, concentration, and ohmic). Numerical results from the Tafel equation and linear current potential were compared with the Butler–Volmer equation. Semiempirical correlations based on experimental kinetic data were also compared to the Butler–Volmer equation. Fick's model, the dusty gas model, and the Stefan–Maxwell model were used to determine the diffusion of reactants into the porous material (concentration polarization). For the ohmic polarization, different expressions of the electrolyte's conductivity were analyzed. Section 3 discusses the results obtained from the macro-level model. The performance characteristics were calculated at different operating conditions and for three electrochemically active fuels (i.e., hydrogen, carbon monoxide and methane). Appendix A describes the formulae required to calculate concentration polarization. A set of rational approximations for the most commonly used binary systems in SOFC technology was included. A sample code implementation of the dusty gas model using Mathematica® is presented in Appendix B.

2. A review of polarization in SOFCs

Let us start by defining the following chemical reaction

$$\nu_A A + \nu_B B \Longleftrightarrow \nu_C C + \nu_D D \tag{1}$$

where the capital letters indicate the chemical constituents and ν the stoichiometric coefficients associated with the balanced reaction.

Based on the definition of Gibbs function: $G \equiv H - TS$, and the fundamental thermodynamic relation: $U = U(S, V, N_A, N_B, N_C, N_D)$, the Gibbs energy for Eq. (1) is given by

$$dG = -S\,dT + V\,dP + (-\nu_A\mu_A - \nu_B\mu_B + \nu_C\mu_C + \nu_D\mu_D)\,d\varepsilon \tag{2}$$

$$dG = -S\,dT + V\,dP + dG_{T,p} \tag{3}$$

where μ represents the chemical potential, and $d\varepsilon$ is a proportionality factor which is always greater than zero; ε is called the degree of reaction or reaction coordinate. It indicates the degree to which the reaction has taken place [19].

The chemical potential (μ) appearing in Eq. (2) (assuming a pure substance in a reactive mixture of ideal gases) [20] is given by

$$\mu = g^o + RT \ln p \tag{4}$$

At equilibrium, any chemical reaction obeys the condition: $dG_{T,p} = 0$. Consequently, combining Eqs. (4) and (2), the equilibrium condition can be expressed in terms of the chemical potential as follows:

$$\nu_C g_C^o + \nu_D g_D^o - \nu_A g_A^o - \nu_B g_B^o = -RT \ln \frac{(p_C)^{\nu_C}(p_D)^{\nu_D}}{(p_A)^{\nu_A}(p_B)^{\nu_B}} \tag{5}$$

The term in the left-hand side is known as the standard-state Gibbs function (ΔG^o). The term in the right-hand side is related to the equilibrium constant (K_p)

$$\Delta G^o = -RT \ln K_p \tag{6}$$

The standard-state Gibbs energy corresponds to the maximum work that can be drawn from a fuel cell that operates at standard conditions. The equilibrium constant can be found in tables or usually is reported in terms of empirical correlations. The partial pressures in Eq. (5) can be expressed in terms of their equivalent mole fractions ($p_i = \chi_i\, p$), thus the equilibrium constant can be rewritten as

$$K_p = \frac{\chi_c^{\nu_C}\chi_D^{\nu_D}}{\chi_A^{\nu_A}\chi_B^{\nu_B}}(p)^{\nu_C+\nu_D-\nu_A-\nu_B} \tag{7}$$

The former set of thermodynamic relations (Eqs. (5)–(7)) are connected with the fuel cell electrochemistry by the reversible open circuit voltage [21]

$$E^o = -\frac{\Delta G^o}{z\mathcal{F}} \tag{8}$$

where E^o is the maximum voltage obtainable from the fuel cell, z the number of electrons transferred, and $\mathcal{F}$ the Faraday constant ($\mathcal{F} = 9.6485 \times 10^4\ \mathrm{C\,mol^{-1}}$).

When off-equilibrium conditions are considered, the partial pressures at equilibrium conditions (Eq. (5)) must be replaced by their actual values. The new ratio represents the off-equilibrium concentrations of reactants and products [22]. Thus the new cell potential in terms of actual concentrations

(off-equilibrium) is given by the well known Nernst equation

$$E = E^{o} - \frac{RT}{n\mathcal{F}} \ln K \tag{9}$$

where K represents the ratio of products to reactants at conditions different from those at equilibrium.

For fuel cells operated with pure hydrogen ($H_2 + \frac{1}{2}O_2 \Longrightarrow H_2O$), the Nernst equation becomes

$$E = E^{o} - \frac{RT}{2\mathcal{F}} \ln \left(\frac{(p_{H_2O})(p)}{(p_{H_2})(\sqrt{p_{O_2}})} \right) \tag{10}$$

The Nernst equation, however, represents an idealized situation. The real voltage has to take into account the losses associated with activation (η_{Ac}), ohmic (η_{Ω}), and concentration polarization ($\eta_{\mathcal{D}}$). Moreover, there are some losses occurring in the fuel cell that cannot be characterized with the above-mentioned polarization terms (for example, leakage), but in general their contribution is insignificant. Maloney [23] studied the influence of different rate-limiting steps in fuel cell performance. Porous gas diffusion, adsorption, surface migration, charge transfer, reaction kinetics, and ohmic resistance were considered. Maloney identified ohmic and activation polarization as the main contributors to irreversibility. For electrolyte-supported cells, the main polarization is attributed to the ohmic loss [24]. For anode-supported cells, ohmic polarization is small because of the thin electrolyte used; therefore, the main contribution comes from activation polarization. Concentration polarization is expected to become an important rate-limiting step at high current densities ($\geq$7500 A m^{-2} for a typical membrane) and low-flow concentrations ($\geq$80% of fuel utilization) [21].

Taking into account the three main sources of irreversibility occurring in the fuel cell, the cell potential is given by

$$E_{Real} = E - \eta_{Ac,A} - \eta_{Ac,C} - \eta_{\Omega,E} - \eta_{\mathcal{D},A} - \eta_{\mathcal{D},C} \tag{11}$$

where the second subscript indicates the polarization at anode (A), cathode(C), and electrolyte (E).

The polarization terms are discussed next. The polarization model assumes that the reactions occur at the electrode–electrolyte interface, no temperature or pressure gradient throughout the electrode thickness, and steady-state conditions.

2.1. Activation polarization

Activation polarization is controlled by the electrode kinetics at the electrode surface. This polarization is directly related to the activation barrier that must be overcome by the reacting species in order for the electrochemical reaction to occur. The electrode reaction rate at high temperatures (600–800 °C) is fast, and the result is that activation polarization is small, which represents the case of SOFCs. Activation polarization is given by the Butler–Volmer equation [25,26]

$$j = j_o \left\{ \exp\left(\frac{\alpha\, \eta_{Ac}\, z\mathcal{F}}{RT} \right) - \exp\left(-\frac{(1-\alpha)\eta_{Ac}\, z\mathcal{F}}{RT} \right) \right\} \tag{12}$$

where j_o is the exchange current density, α the electron transfer coefficient, and z the number of electrons transferred per reaction. The exchange current density is influenced by different factors which are not clearly understood [12]. Semiempirical correlations based on experimental data are usually used for the exchange current density; however, Campanari et al. [27] showed that reported values in the literature can vary widely. For our calculations we used recommended values by Chan et al., but we recognize that more work needs to be done on this area. The electron transfer coefficient depends on the electrocatalytic reaction mechanism and typically takes values between zero and one.

The Butler–Volmer equation is solved numerically in this paper. The most commonly used method for solving non linear equations is the Newton–Raphson. The MatLab® fzero function uses the *zeroin* algorithm for solving nonlinear equations. The *zeroin* algorithm combines bisection, quadratic interpolation, and secant methods for speed and reliability. An improved version of this algorithm was developed by Moler [28]. The Mathematica® FindRoot function uses Newton, secant, and Brent's methods for finding a solution to non-linear equations. Both algorithms were used for this paper.

At high-activation polarization, the second term in the Butler–Volmer equation will be much smaller compared to the first term and can be eliminated. The resulting expression is the well known Tafel expression

$$\eta_A = \frac{RT}{\alpha\, z\mathcal{F}} \ln\left(\frac{j}{j_o} \right) \tag{13}$$

At low-activation polarization, the term $(\alpha\, z\mathcal{F}\eta_A)/RT$ will be much less than unity and the exponential can be expanded as a Taylor series

$$j = j_o \left\{ \frac{z\mathcal{F}\eta_A}{RT} + \left(-\frac{1}{2} + \alpha \right) \left(\frac{z\mathcal{F}\eta_A}{RT} \right)^2 + \bigcirc \left[\frac{z\mathcal{F}\eta_A}{RT} \right]^3 \right\} \tag{14}$$

Neglecting all terms with an order higher than one, and solving for η_A, the well known linear current potential relation is obtained

$$\eta_A = \frac{RT}{z\mathcal{F}\, j_o} j \tag{15}$$

Whether to use the full Butler–Volmer equation or its simplified forms depends on the accuracy desired and the expected activation polarization. Table 1 shows the ranges at which the Tafel and the linear current potential are within a 5% error relative to the Butler–Volmer equation. These ranges were calculated from correlated linear expressions (see Eqs. (16) and (17)), which correspond to the fitted values at which the ratio j/j_o gives an error of 5% (Fig. 1) compared to the Butler–Volmer expression. Table 1 is in good agreement with the values reported by Chan et al. [11], but the results presented here in the form of correlated expression gave us

Table 1
Activation polarization range for 5% accuracy of simplified models relative to the Butler–Volmer equation

T (K)	Tafel, η_A	Linear current potential, η_A
1073	≥0.2516	≤0.1006
1173	≥0.2751	≤0.1100
1273	≥0.2985	≤0.1194
1373	≥0.3219	≤0.1287
1473	≥0.3454	≤0.1382

more information than the previous results presented by Chan et al. at only one temperature.

Tafel error correlation:

$$\eta_A \geq 0.0002345\,T - 8.06497 \times 10^{-7} \quad (16)$$

Linear current potential:

$$\eta_A \leq 0.0000938\,T - 4.483069 \times 10^{-7} \quad (17)$$

2.2. Empirical correlations for the activation loss

It is common to use semiempirical correlations to calculate the polarization occurring in the fuel cell. These correlations are preferred because of their simplicity; however, their accuracy is questionable in a wide range of operating conditions. The most widely used correlations are the ones reported by Achenbach [15]

Cathode:

$$\frac{1}{R_C} = \frac{4\mathcal{F}}{RT} r_C \left(\frac{p_{O_2}}{p}\right)^m \exp\left(-\frac{E_C}{RT}\right) \quad (18)$$

Anode:

$$\frac{1}{R_{A,H_2}} = \frac{2\mathcal{F}}{RT} r_{A,H_2} \left(\frac{p_{H_2}}{p}\right)^m \exp\left(-\frac{E_A}{RT}\right) \quad (19)$$

$$\frac{1}{R_{A,CO}} = \frac{2\mathcal{F}}{RT} r_{A,CO} \left(\frac{p_{CO}}{p}\right)^m \exp\left(-\frac{E_A}{RT}\right) \quad (20)$$

where $p_{O_2} = 0.21p$, $p_{H_2} = 0.50p$, $p_{CO} = 0.01p$, $E_C = 160\,\mathrm{kJ\,mol^{-1}}$, $E_A = 110\,\mathrm{kJ\,mol^{-1}}$, $r_C = 1.489 \times 10^{10}$ $\mathrm{A\,m^{-2}}$, $r_{A,H_2} = 2.128 \times 10^8\,\mathrm{A\,m^{-2}}$, and $r_{A,CO} = 2.98 \times 10^8\,\mathrm{A\,m^{-2}}$; the preexponential factors were calculated under the assumption of $R = 0.1\,\Omega\,\mathrm{cm^2}$. The preexponential factors were calculated at 1000 °C; therefore better predictions are expected near this temperature. Achenbach's correlations were calculated from experimental kinetic data assuming low polarization. A quantitative comparison between three different empirical correlations, including Achenbach's expressions, was reported by Motloch [22]. A summary of Motloch's correlations is presented in Table 2. The total or equivalent resistance is calculated considering the fuel cell being analogous to an electrical circuit, where the cathode and the anode are connected in series. If carbon monoxide and hydrogen are considered electrochemically active fuels, then the equivalent resistance is calculated viewing the fuels as being in parallel: $R^{-1} = R_{A,H_2}^{-1} + R_{CO}^{-1}$. Motloch found that the variation among the three models is minimal at high temperatures, $T \geq 1000\,^\circ\mathrm{C}$; however, at lower temperatures, $T \leq 800\,^\circ\mathrm{C}$, these expressions produced unrealistic results. For example at 800 °C (typical value for the SOFC operating temperature), the overpotential is $\eta = 1.0578\,\mathrm{V}$, assuming a current density of $7500\,\mathrm{A\,m^{-2}}$.

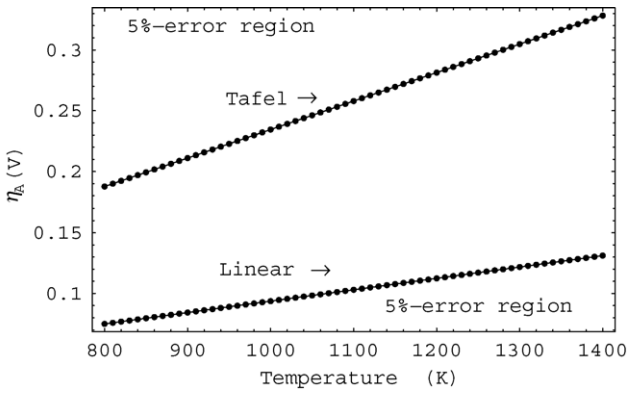

Fig. 1. Operating region for Tafel and linear current potential as function of temperature and activation polarization for a 5% error relative to the Butler–Volmer equation.

Table 2
Resistance correlations for calculating the activation polarization; $R = r\exp(E/T)$

Reference	Region	r ($\Omega\,\mathrm{m^2}$)	E (K)
Achenbach	Cathode	2.72×10^{-12}	19244
	Anode (H_2)	3.07×10^{-10}	13230
	Anode (CO)	5.82×10^{-10}	13230
Hendriksen	Cathode	9.02×10^{-13}	20882
	Anode	1.35×10^{-8}	8121
Karoliussen	Anode and cathode	2.83×10^{-8}	8360

A comparison between these correlations and the Butler–Volmer equation reveals that the empirical correlations were reasonably accurate between 900 and 1473 °C (1173 and 1273 K) (Figs. 2 and 3). At higher temperatures, the empirical expressions gave polarization values much smaller than the Butler–Volmer equation, which was expected based on the assumptions used for these correlations. However, at lower and higher temperatures ($T \leq 900\,^\circ\mathrm{C}$ and $T \geq 1473\,^\circ\mathrm{C}$), the numerical values reported unrealistic results and cannot be used for any practical purpose. Based on our numerical findings, we recommend the use of the full Butler–Volmer equation and avoid the use of semiempirical correlations, especially at low temperatures. Although the Tafel and the linear current potential could simplify computational time in the past, today the implementation of algorithms for solving systems of algebraic non-linear equations is fast enough, and there is no reason to sacrifice accuracy for simplified relations.

2.3. Concentration polarization

Concentration polarization occurs when the fuel is consumed at the electrode–electrolyte interface, and the gas con-

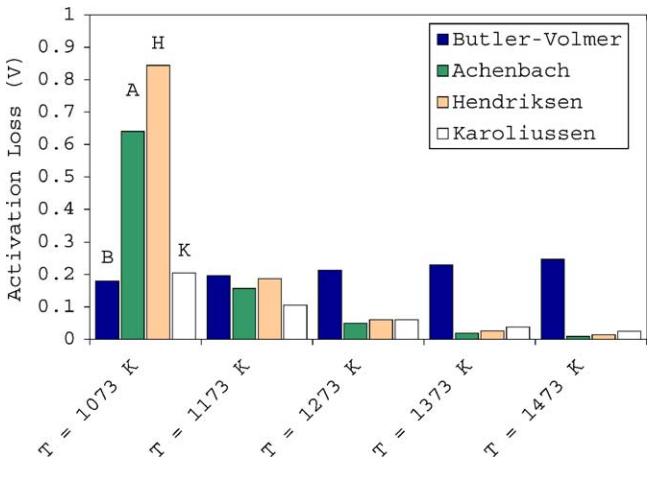

Fig. 2. Comparison between the total activation polarization using the Butler–Volmer equation (B) and empirical correlations reported by Achenbach [15] (A), and Motloch [22] (H = Hendriksen, K = Karoliussen); current density $j = 3000\ \mathrm{A\,m^{-2}}$ and exchange current density based on recommended values by Chan et al. [11].

centration decreases at the reaction sites. Concentration polarization becomes an important loss at high current densities and small fuel concentrations (≥80% of fuel utilization). The main factors that contribute to concentration polarization are diffusion of gases through the porous media and solution–dissolution of reactants and products. The transport mechanisms within the fuel cell are governed by diffusion transport and Darcy's viscous flow. For typical operating conditions on an SOFC, diffusion transport will dominate and convection transport can be neglected (Darcy's flow). Molecular diffusion and Knudsen diffusion describe the diffusion transport through the porous electrode. Their contribution to diffusion transport is tightly related to the microphysical characteristics of the porous material (i.e., porosity, tortuosity, pore size,

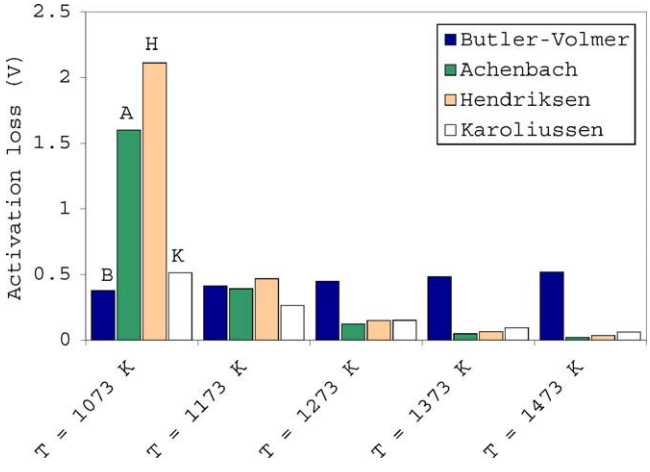

Fig. 3. Comparison between the total activation polarization using the Butler–Volmer equation (B) and the empirical correlations reported by Achenbach [15] (A) and Motloch [22] (H = Hendriksen, K = Karoliussen); current density $j = 7500\ \mathrm{A\,m^{-2}}$ and exchange current density based on recommended values by Chan et al. [11].

and permeability). The diffusion transport in a porous material can be described by Fick's model, the dusty gas model or the Stefan–Maxwell model. Fick's model is used more frequently because it is simpler to implement than the dusty gas model and analytical expressions can be derived more easily [29]; the Stefan–Maxwell model is usually discarded because it does not include Knudsen diffusion. If Knudsen diffusion is dominant, the dusty gas model predictions are more accurate than those from Fick's model [30]. The reason is attributed to the way the overall effective diffusion coefficients are determined in both models.

2.3.1. Fick's model

The mass transport equation of a single component fluid is described by

$$\frac{\varepsilon}{RT}\frac{\partial(y_i P)}{\partial t} = -\nabla \cdot N_i + r_i \tag{21}$$

where ε is the porosity, N_i the rate of mass transport, and r_i the reaction rate in the porous electrode [29]. Assuming the process occurs at steady state and that the electrochemical reaction takes place at the anode–electrolyte interface the mass transport equation becomes

$$\nabla \cdot N_i = 0 \tag{22}$$

Fick's model is given by

$$N_i = \frac{1}{RT}\left(-\mathcal{D}_{\mathrm{a,e}}\frac{\partial(y_i P)}{\partial z}\right) \tag{23}$$

where $\mathcal{D}_{\mathrm{a,e}}$ is the overall effective diffusion coefficient (see Appendix A).

For the binary system, H_2–H_2O, the rate of mass transport as given by Fick's model is

$$N_{\mathrm{H_2}} = -\frac{\mathcal{D}_{\mathrm{a,e}}}{RT}\frac{\partial(y_{\mathrm{H_2}} P)}{\partial z} \tag{24}$$

At the anode–electrolyte interface ($z = \ell$) the current density produced is governed by the rate of reactant diffusing into the porous anode by

$$N_{\mathrm{H_2}} = \frac{j}{2\mathcal{F}} \tag{25}$$

substituting this value into Eq. (24), the following boundary condition is obtained:

$$\left.\frac{\partial y_{\mathrm{H_2}}}{\partial z}\right|_{z=\ell} = -\frac{RT}{2P\,\mathcal{F}\mathcal{D}_{\mathrm{a,e}}} j \tag{26}$$

By solving the mass transport equation for the system, H_2–H_2O (Eq. (24)) with boundary conditions, Eq. (26) and $y_{\mathrm{H_2}}(z=0) = y_{\mathrm{H_2}}^{\mathrm{Bulk}} = y_{\mathrm{H_2}}^{\mathrm{I}}$, the composition of the binary system can be computed at the electrode–electrolyte interface

$$\frac{\partial}{\partial z}\left(-\frac{\mathcal{D}_{\mathrm{a,e}}\,P}{RT}\frac{\partial y_{\mathrm{H_2}}}{\partial z}\right) = 0 \tag{27}$$

$$p_{H_2} = p^{I}_{H_2} - \frac{RT}{2\,\mathcal{F}\mathcal{D}_{a,e}} j\,z \tag{28}$$

Noticing that $p_{H_2} + p_{H_2O} = 1$

$$p_{H_2O} = p^{I}_{H_2O} + \frac{RT}{2\,\mathcal{F}\mathcal{D}_{a,e}} j\,z \tag{29}$$

The concentration at the interface is therefore calculated in terms of the partial pressures of the species involved, hydrogen in this case. In general, for any system containing a binary component system the diffusion transport, according to Fick's model, is given by Eq. (28); the 2 in the denominator has to be modified in terms of the number of electrons transferred when different systems are considered. The Stefan–Maxwell model is applied if Knudsen diffusion is assumed to be insignificant. In this case, the same procedure developed for Fick's model is used, with the only difference being that the overall effective diffusion coefficient ($\mathcal{D}_{a,e}$) does not include Knudsen diffusion. The analytical treatment of multicomponent systems using Fick's model becomes excessively complex (from a mathematical point of view) for systems greater than three components, and numerical models are used instead [31].

2.3.2. Dusty gas model

The dusty gas model (DGM), similar to Fick's model, includes molecular diffusion and Knudsen diffusion but is based on the Stefan–Maxwell formulation. The rate of mass transport according to the DGM is given by

$$\frac{N_i}{\mathcal{D}_{k,e}} + \sum_{j=1,j\neq i}^{n} \frac{y_j N_i - y_i N_j}{\mathcal{D}_{ij,e}} = -\frac{P}{RT}\frac{dy_i}{dz} \tag{30}$$

The DGM assumes that the pore walls consist of giant, motionless, pseudo molecules (dust) that are uniformly distributed in space. The flux ratio is determined using the Graham's law of diffusion in gaseous mixtures whereas in Fick's model an equimolar counter diffusion concept is used instead. The DGM is more accurate when Knudsen diffusion is dominant, because at these conditions the assumption of equimolar counter diffusion is no longer valid [30].

Using the DGM, the compositions for the system, H_2–H_2O, at the electrode–electrolyte interface, are given by

$$y_{H_2} + y_{H_2O} = 1 \tag{31}$$

$$\frac{d^2 y_{H_2}}{dz^2} + \frac{\alpha}{\mathcal{D}_{H_2-H_2O,e}}\left\{\frac{1-\alpha\,y_{H_2}}{\mathcal{D}_{H_2-H_2O,e}} + \frac{1}{\mathcal{D}_{H_2,k,e}}\right\} \times \left(\frac{dy_{H_2}}{dz}\right)^2 = 0 \tag{32}$$

with the following boundary conditions:

$$y_{H_2}(0) = y^{I}_{H_2} \tag{33}$$

$$\left.\frac{dy_{H_2}}{dz}\right|_{z=0} = -j\frac{RT}{2p\mathcal{F}}\left\{\frac{1-\alpha\,y^{I}_{H_2}}{\mathcal{D}_{H_2-H_2O,e}} + \frac{1}{\mathcal{D}_{H_2,k,e}}\right\} \tag{34}$$

where

$$\alpha = 1 - \sqrt{\frac{M_{H_2}}{M_{H_2O}}}$$

The derivation for ternary systems was presented by Suwanwarangkul et al. [30]. In this paper, the DGM for multicomponent systems is implemented assuming no convection transport and that all molar fluxes are known from the global electrochemical reactions. Although the assumption of no convection transport could limit the usability of the method in some cases, it considerably reduces its complexity for computational purposes. For instance, the method proposed by Zhu and Kee [12] requires an iterative procedure for solving the DGM, while the derivation of analytical expressions becomes very complicated for multicomponent systems. Using the assumption of constant pressure, our results (multicomponent systems) are quantitatively comparable to those reported by others [12], while the problem can be easily treated from a computational point of view.

2.3.3. Numerical calculations of concentration polarization

Concentration polarization is defined as the difference between the ideal and real cell voltage (when corrected for ohmic and activation polarizations). The ideal voltage is calculated in terms of the bulk concentration in the stream channel, whereas the real cell voltage is calculated at the electrode–electrolyte interface. For the binary system, H_2–H_2O, the concentration polarization is given by

$$\eta_C = -\frac{RT}{2\mathcal{F}}\ln\left(\frac{y_{H_2}\cdot y^{I}_{H_2O}}{y_{H_2O}\cdot y^{I}_{H_2}}\right) \tag{35}$$

where the superscript I indicates inlet conditions.

Fick's model, DGM and the Stefan–Maxwell model were implemented with Mathemathica®,[1] and the results are presented next. The physical parameters of the porous electrodes (i.e., porosity and tortuosity) are determined from recommended values by other authors [17,32,33]. The overall diffusion coefficient is calculated first; afterwards, one of the three models is implemented. Finally, the resulting flow concentration (usually in terms of partial pressures) is used together with the definition of concentration polarization.

These calculations were useful to identify some features of the system behavior to diffusion transport. The first important feature was the sensitivity to flow concentration. The shape of the concentration polarization changed from concave-down to concave-up at high- and low-flow concentration, respectively (Figs. 4 and 5). This indicates that at low-flow concentrations the diffusion effects became more important than at higher-flow concentrations. The limiting current at 50% of fuel utilization and 800 °C was found at

[1] The algorithms used for these calculations are available, at no cost, at: http://uweb.und.nodak.edu/~eduardo.hernandez.pacheco/Performance.htm.

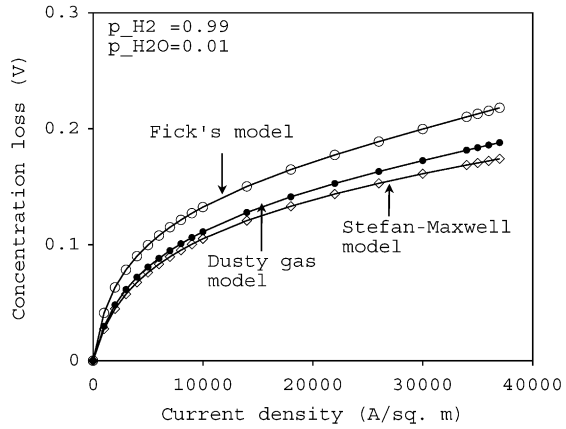

Fig. 4. Anode concentration polarization for an anode-supported cell using Fick's (○), dusty gas (●) and Stefan–Maxwell (◇) models. Anode thickness $\delta = 750 \times 10^{-6}$ m, $T = 800\,^{\circ}$C.

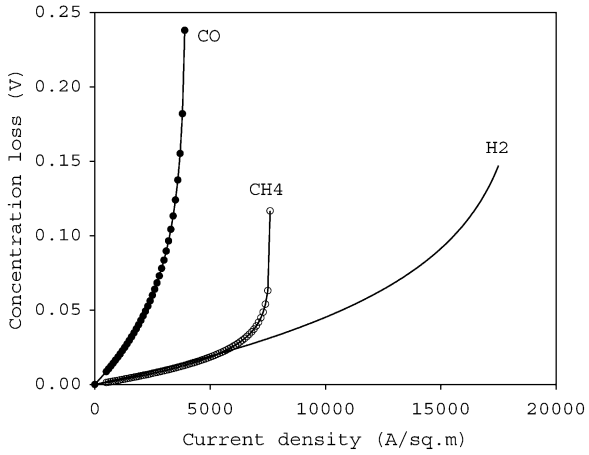

Fig. 6. Concentration polarization at 80% of fuel utilization considering the direct oxidation of hydrogen (—), methane (○), and carbon monoxide (●). Anode thickness $\delta = 600 \times 10^{-6}$ m, $T = 950\,^{\circ}$C.

approximately 35 000 A m^{-2} (Fig. 5). At high-flow concentrations the DGM and the Stefan–Maxwell model reported similar results (Fig. 4); however at low-flow concentrations, the Stefan–Maxwell model gave poor predictions with respect to the other two models (Fig. 5). If methane and carbon monoxide are considered electrochemically active fuels, the diffusion transport will play an important role in determining the performance characteristics. At low-flow concentration (80% fuel utilization), the diffusion transport of methane and carbon monoxide became noticeably lower than that for hydrogen (Fig. 6). Lower values of the limiting current will be obtained with heavier compounds because diffusion to the reaction sites becomes more important. This indicates that although higher power densities can be reached with some hydrocarbons, concentration polarization will be an important source of irreversibility. These numerical results revealed diffusion problems with fuel cells operated with heavy molecules.

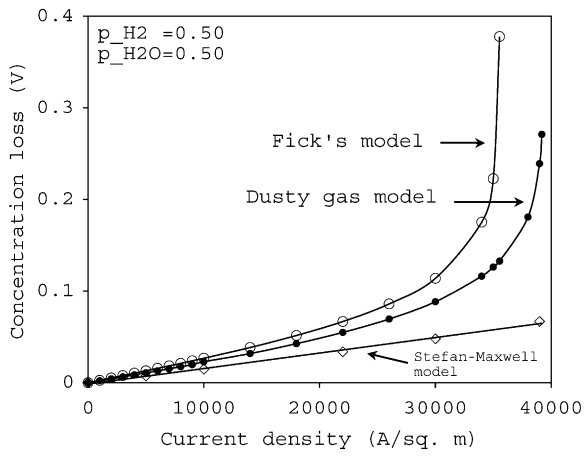

Fig. 5. Anode concentration polarization for an anode-supported cell using Fick's (○), dusty gas (●) and Stefan–Maxwell (◇) models. Anode thickness $\delta = 750 \times 10^{-6}$ m, $T = 800\,^{\circ}$C.

Based on the recommendations given by Suwanwarangkul et al. and the results shown here, we concluded that the DGM is more accurate for predicting the concentration polarization and, therefore, was the method chosen for our performance calculations.

2.4. Ohmic polarization

Ohmic resistance polarization occurs in the electrode materials (anode and cathode), interconnects, and in the electrolyte. This loss is the resistance to the flow of electrons in the electrodes and ions in the electrolyte. The ohmic loss is perhaps the major loss mechanism in an electrolyte-supported fuel cell [24]. For anode-supported cells, this polarization will not have a big effect on the cell's performance. The electrode ohmic polarization is not taken into account because of the high conductivity of the electrodes; therefore, the dominant ohmic loss is that for the electrolyte. Ohmic polarization obeys Ohm's law and is given by

$$\eta_{\Omega} = j\,R_{\Omega} \tag{36}$$

where R_{Ω} represents the total ionic and electronic resistance (expressed in terms of the resistivity of each material, $R_{\Omega} = \varphi\,L$) and j is the current density. The resistivity of the different materials that integrate the fuel cells is required in Eq. (36). A summary of commonly used empirical correlations for determining the conductivity and resistivity of Ni-YSZ is presented in Table 3 [22,34,35].

Table 3
Resistivity φ (Ω cm) and electrical conductivity σ (Ω^{-1} cm^{-1}) parameters for YSZ

A	B	Equation
$7.86 \times 10^5/T$	−10556	$A + \exp(B/T)$
190	−9281	$A + \exp(B/T)$
334	−10300	$A + \exp(B/T)$
0.3685	10300	$(A + 0.002838\,\exp(B/T))^{-1}$
0.00294	10350	$(A\,\exp(B/T))^{-1}$

These correlations showed an almost perfect agreement at medium temperatures (≈600 °C) and a small discrepancy at high temperatures (>900 °C). The variation of these correlations could be attributed to the different composition used in the electrolyte. We have chosen the correlation reported by Bessette because of its consistency with the other correlations in the entire range analyzed and its simplicity.

3. Results

The performance of the fuel cell was determined using the macro-level model. For pure electronic conductors as electrodes, it is logical to assume that the reactions take place at the electrode–electrolyte interface. However, for composite electrodes as Ni-YSZ (cermet), a micro-level model will be required. Although the assumption of a pure electronic conductor does not apply to cermet electrodes, the numerical results reported by Chan et al. [11] showed that for anode-supported cells with thick anodes (≥600 μm), the main contribution to polarization occurred near the interface. The SOFC membranes modeled in this paper have anodes of 600–750 μm. This anode thickness corresponds to values found in commercial membranes that are being investigated at the EERC and UND for the BG-SOFC system. Porosity and tortuosity can be determined experimentally; however, recommended values were used for this model. Corrected values of these parameters will be determined from performance experiments in future work; these parameters can be corrected in order to fit the performance curves obtained experimentally. The algorithm to compute the polarization in the SOFC proceeds as follows. The activation polarization was calculated using the Butler–Volmer equation. The *zeroin* algorithm was used in this paper, the exchange current density was based on values recommended by Chat et al. and Zhu and Kee. The DGM was implemented for determining the diffusion transport in the anode. The numerical values for the cathode electrode were found insignificant compared to those at the anode. A sample code is presented in Appendix B to determine the concentration polarization at the interface of a binary system. The dusty gas model requires the knowledge of the fuel composition at the bulk stream. This composition was determined based on the fuel utilization desired. The ohmic polarization resistance was calculated using a semiempirical correlation reported by Bessette. At the electrodes, an insignificant resistance is expected because of the high conductor material. The algorithm permitted us to investigate the optimal operating conditions for optimal performance.

The macro-level model was implemented on a membrane operated at 80% of fuel utilization and 800 °C. The fuel is assumed to be pure hydrogen. The maximum power was obtained at approximately 3600 W m^{-2} and a current density of 9600 A m^{-2} (Fig. 7). At this value, the polarization contribution was distributed as follows: (1) cathode activation polarization (0.2976 V), (2) anode activation polarization (0.1503 V), (3) ohmic polarization (0.0436 V) and (4) anode concentration polarization (0.0385 V). The cathode activation polarization reported the highest values because of the low exchange current density used ($j_o = 200$ A m^{-2}). Although anode concentration polarization did not represent an important loss at this current density, at higher values, this polarization increased very rapidly, especially near the limiting current density of 18 000 A m^{-2}. Fuel utilization is tightly related to the concentration polarization, because more fuel is demanded at high fuel utilization, more concentration polarization is expected. Fuel cells usually operate at 70–80% of fuel utilization for a compromise between performance and operational costs. Because of the thin electrolyte used (10 μm), ohmic polarization had the smallest contribution to the voltage loss, but for different types of cells (electrolyte-supported cells), this polarization represents the main factor for reducing the performance of the cell.

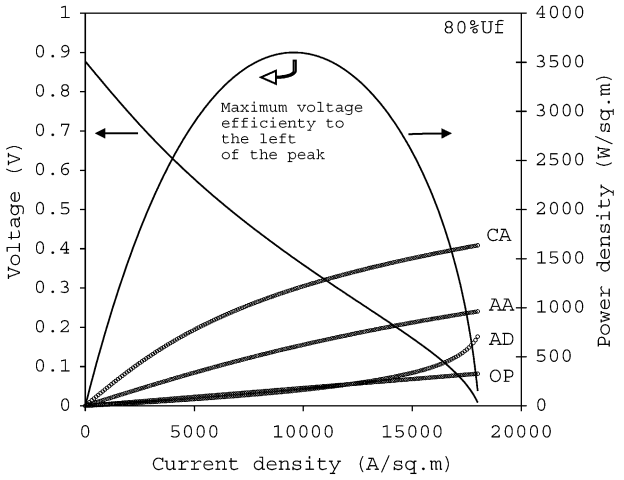

Fig. 7. Performance characteristics for hydrogen at 80% of fuel utilization and 800 °C. Cathode activation polarization (CA), anode activation polarization (AC), anode concentration polarization (AD) and electrolyte-ohmic polarization (OP).

Temperature also plays an important role in determining the performance characteristics of the fuel cell. As Fig. 8 shows, the maximum power density shifted to a lower value when the temperature decreased. The performance-jump from 800 to 700 °C was smaller than the jump from 700 to 600 °C. The main reason for this is because at low temperatures, both ohmic polarization and concentration polarization reported higher values of voltage loss (Fig. 9(a) and (b)). This is especially notorious for ohmic polarization. At low values of temperature and high values of current density, the ohmic polarization increased more rapidly than the other losses. Consequently, the change in power density at 600 °C had a bigger impact than the change at higher temperatures (700–800 °C). At high temperatures (>700 °C) the main contribution to voltage loss came from activation polarization (Fig. 9(c) and (d)). As temperature and current density increased, the activation polarization also increased but not as drastically as the ohmic polarization did at low temperatures (≈600 °C).

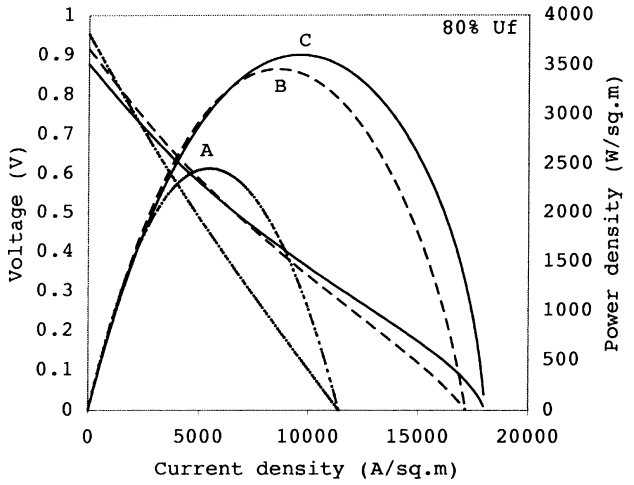

Fig. 8. Performance characteristics for hydrogen at 80% of fuel utilization and different temperatures. (A) $T = 600\,^{\circ}\mathrm{C}$, (B) $T = 700\,^{\circ}\mathrm{C}$, (C) $T = 800\,^{\circ}\mathrm{C}$.

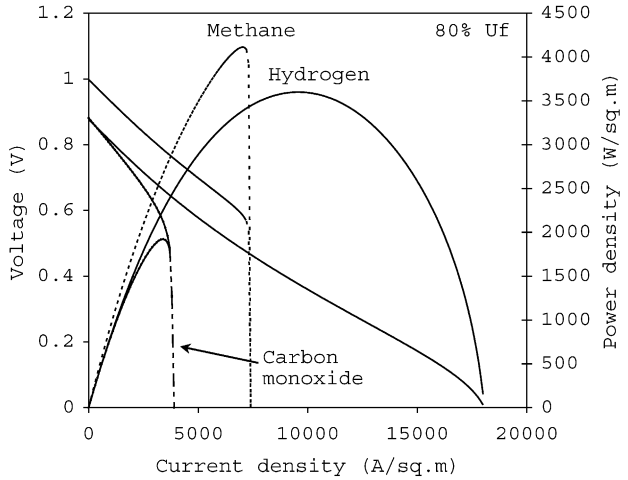

Fig. 10. Performance characteristics of three electrochemically active fuels: hydrogen, methane, and carbon monoxide. The numerical calculations were made at 80% of fuel utilization.

The effect of using different electrochemically active fuels is investigated next. Although the direct oxidation of hydrocarbons is not possible to date with conventional Ni-YSZ anodes, there are many research groups developing new anode materials because of the abundant benefits of this technology [36]. As mentioned before, the gases leaving the gasifier will be composed of hydrogen, methane, carbon monoxide, carbon dioxide, and small amount of tars (1–5%) [3]. Methane is more likely to reform into hydrogen and carbon monoxide rather than being directly oxidized. Carbon monoxide can be directly oxidized on Ni-YSZ anodes but the water–gas shift reaction is more favorable in the presence of water. The detailed understanding of all the different reaction mechanisms that occur in the fuel cell is fundamental for a complete analysis of the performance characteristics of a fuel cell. However, for a generic analysis, some simplifications can be made. For instance, for a H_2–CO system, the water–gas shift reaction is assumed to be always at equilibrium and hydrogen can be considered the only fuel in the system [37]. For a more complex system like natural gas (85% methane), the methane can be assumed to be internally reformed at high temperatures (500–800 °C), and the reaction rates will determine the amount of hydrogen being produced in the system [38]. Fig. 10 shows the performance obtained from a hypothetical fuel cell operated with pure methane and pure carbon monoxide. The benefits obtained from a higher Nernst potential in the case of methane are rapidly overshadowed by diffusion

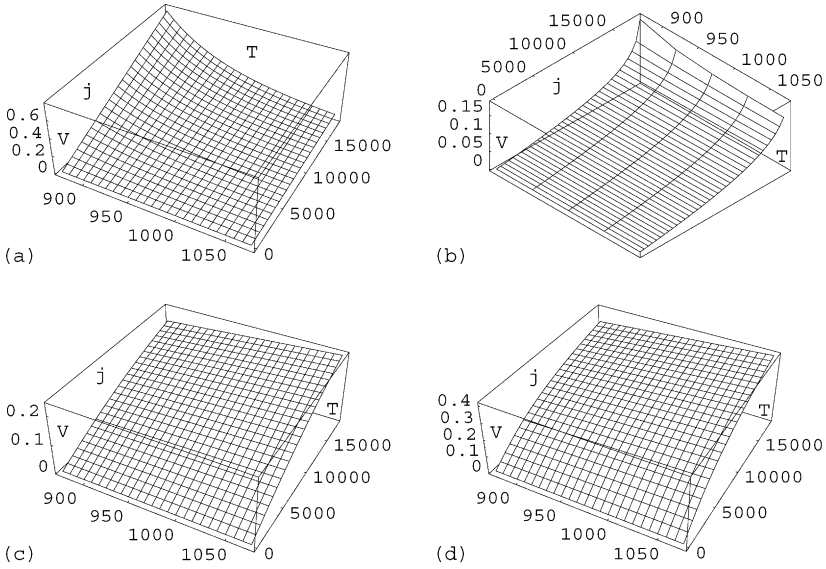

Fig. 9. Polarization curves (V [V]) as a function of temperature (T [K]) and current density (j [A m^{-2}]) for hydrogen at 80% of fuel utilization. (a) Ohmic polarization, (b) concentration polarization, (c) anode activation polarization, and (d) cathode activation polarization. Current density = 0–18 000 A m^{-2}, temperature = 600–800 °C (800–1073 K).

problems (concentration polarization). The window of operation for this hypothetical cell will be small. Although the benefits of this technology (direct oxidation of hydrocarbons) are vast, new problems will arise. For now, internal reforming and partial oxidation will be a more feasible technology for the use of hydrocarbons in SOFCs [39].

4. Final remarks

A macro-level model was used to determine the performance characteristics of an anode-supported cell. The Butler–Volmer equation was recommended for the activation polarization; however, for simplified models (Tafel and linear current potential), ranges of 5% error relative to the Butler–Volmer equation were reported in the form of two correlated expressions. Concentration polarization was calculated using the DGM. An algorithm of this model implemented on a binary component system is included in this paper. For multicomponent systems the algorithms are available from the authors. Cathode concentration polarization was not included because the diffusion transport contribution was insignificant because of the thin cathode used (40 μm). For the ohmic polarization, different empirical correlations showed minimal variation, especially at SOFC operating temperatures (600–800 °C). The contribution to voltage loss was analyzed for hydrogen at 80% of fuel utilization and 800 °C on a anode-supported cell. A surface chart for each polarization term as functions of temperature and current density was presented. The model was also implemented for carbon monoxide and methane, assuming they were electrochemically active fuels. The results showed that concentration polarization will be an important problem associated with this technology. Our objective was to provide a set of simple computational tools for calculating the performance characteristics of an SOFC and determining the operating conditions for optimal performance. Fuel cells usually operate to the left of the maximum power density, because of the better voltage efficiency and stability of the membrane. However, at low current densities (left of the peak power density) carbon deposition is expected (for the case of dry methane or low water content), which will limit the window of operating conditions. This analysis and the tolerance of SOFCs to tars is being investigated at the EERC and will be presented in the future. Our results showed the operating conditions at which the optimal performance is obtained. However, in reality, the optimal performance is a compromise among maximum power density, operational stability, and capital costs.

Acknowledgement

This material is based upon work supported by the National Science Foundation under grant No. 0093923. We would also like to acknowledge Xcel Energy for its generous support.

Appendix A. Diffusion coefficients

Diffusion in porous media is usually described by molecular diffusion or Knudsen diffusion. Knudsen diffusion occurs when the diameter pores are small compared with the mean free path of the gas molecules. Ordinary diffusion occurs when the pore diameter is large compared with the mean free path of the gas molecules. The mean free path represents an average of the distance that the molecules can travel before a collision occurs. The Knudsen number $K_n = \lambda/d$ (where λ is the mean free path length and d the pore diameter) characterizes the diffusion process. For $K_n \ll 1$ ordinary diffusion dominates, for $K_n \gg 1$ Knudsen diffusion dominates. For SOFCs, both Knudsen and ordinary diffusion processes have to be considered since, in general, $K_n \approx 1$.

For straight and round pores [11], Knudsen diffusion is given by

$$\mathcal{D}_{i,k} = \frac{2}{3} r \sqrt{\frac{8000\,R\,T}{M_i}} \tag{A.1}$$

$$r = \frac{2\varepsilon}{S_{\mathrm{A}}\rho_{\mathrm{B}}} \tag{A.2}$$

where S_{A} is the surface area of the porous solid ($\mathrm{m^2\,kg^{-1}}$), ρ_{B} the bulk density of the solid particle ($\mathrm{kg\,m^{-3}}$), ε the porosity material, and M the molecular mass ($\mathrm{kg\,kmol^{-1}}$).

In order to account for the tortuosity of the material, the Knudsen coefficient has to be modified in terms of an effective coefficient [11,12]:

$$\mathcal{D}_{i,k,\mathrm{e}} = \mathcal{D}_{i,k}\left(\frac{\varepsilon}{\xi}\right) \tag{A.3}$$

$$\mathcal{D}_{i,k,\mathrm{e}} = \frac{4}{3} r \frac{\varepsilon}{\xi} \sqrt{\frac{8RT}{\pi\,M_i}} \tag{A.4}$$

where ε/ξ represents the porosity:tortuosity ratio. Zhang et al. [32] proposed a new way to predict tortuosity in catalyst pellets based on fractal geometries; a hard spheres model is often used for determining tortuosity. The accurate determination of this parameter is out of the scope of this paper and a recommended values of 2.0–6.0 were used instead.

The binary diffusion coefficients can be determined from the Chapman–Enskog theory [40]

$$\mathcal{D}_{i,j} = \frac{3}{16} \frac{\sqrt{4\pi\,kT/M_{ij}}}{n\pi\,\sigma_{i,j}^2 \Omega_{\mathrm{D}}} \tag{A.5}$$

If gases are assumed to be ideal, the former equation can be simplified to

$$\mathcal{D}_{i,j} = \frac{0.0026\,T^{3/2}}{p\,M_{i,j}^{1/2}\,\sigma_{i,j}^2\,\Omega_{\mathrm{D}}} \tag{A.6}$$

where f_{D} is assumed to take a value of one, and n is determined using the ideal gas law. When using these equations,

Table A.1
Lennard–Jones potentials

	N_2	O_2	CH_4	H_2O	CO	H_2	CO_2
σ_i	3.798	3.467	3.758	2.641	3.690	2.827	3.941
ε_i/k	71.400	106.700	148.600	809.100	91.700	59.700	195.200

Table A.2
Collision integral constants

A	*B*	*C*	*D*	*E*	*F*	*G*	*H*
1.06036	0.15610	0.19300	0.47635	1.03587	1.52996	1.76474	3.89411

the following observations have to be considered:

$$M_{i,j} = 2 \times \left(\frac{1}{M_i} + \frac{1}{M_j} \right)^{-1} \tag{A.7}$$

$$\sigma_{i,j} = \frac{\sigma_i + \sigma_j}{2} \tag{A.8}$$

$$\Omega_D = \frac{A}{\tau^B} + \frac{C}{\exp(D\tau)} + \frac{E}{\exp(F\tau)} + \frac{G}{H\tau} \tag{A.9}$$

$$\tau = \frac{kT}{\varepsilon_{i,j}} \tag{A.10}$$

$$\varepsilon_{i,j} = (\varepsilon_i \varepsilon_j)^{1/2} \tag{A.11}$$

where $k = 1.38066 \times 10^{-23}$ ($J\,K^{-1}$) is the Boltzmann's constant, $\sigma_{i,j}$ (Å) the characteristic length, $\varepsilon_{i,j}$ (K) the characteristic Lennard–Jones length, and Ω_D the collision integral based on the Lennard–Jones 12–6 potential. Values for the characteristic lengths are reported in Table A.1 and the constants appearing in the collision integral are reported in Table A.2 (taken from Reid et al. [40]).

Similar to the effective Knudsen coefficient, the binary diffusion coefficient has to be modified in order to account for the tortuosity of the material,

$$\mathcal{D}_{i,j,e} = \mathcal{D}_{i,j} \left(\frac{\varepsilon}{\xi} \right) \tag{A.12}$$

Because ordinary and Knudsen diffusion might occur simultaneously an overall effective diffusion coefficient is given by

$$\frac{1}{\mathcal{D}_{a,e}} = \frac{\xi}{\varepsilon} \left(\frac{1}{\mathcal{D}_{i,j}} + \frac{1}{\mathcal{D}_{i,k}} \right) \tag{A.13}$$

Todd et al. [41] compared different approximations for the determination of molecular diffusion for binary systems. The approximations were compared with the scarce experimental data available. He recommended the Fuller et al. [40] method because it was consistently accurate over the entire temperature range analyzed. Based on this method, Table A.3 contains a set of rational approximations for the binary diffusion on a system that contains H_2, H_2O, CO, CO_2 and CH_4; the method of rational approximation has been used previously for the determination of thermophysical properties of gases [42,43].

$$\mathcal{D}_{i,j} = \frac{a_0 + a_1 T + a_2 T^2}{1 + b_1 T}$$

Appendix B. Dusty gas model (sample code)

The dusty gas model (DGM) for a binary component system (H_2–H_2O) was implemented using Mathematica®. The fuel utilization is set to 80% for three current densities (3000, 7500, and 15 000 A m^{-2}) and a thickness anode of 600 μm. The diffusion coefficients are calculated using the method proposed by Fuller et al. [40]. The concentration polarization is calculated once the diffusion values are known (last line of code).

Table A.3
Binary diffusion coefficients as function of temperature

	a_0	a_1	a_2	b_1	R^2	SSE
H_2–H_2O	−0.152275	0.001572	7.031465e-06	0.000109	0.9999	0.001755
H_2–CO	−0.131687	0.001363	6.114805e-06	0.000109	0.9999	0.001515
H_2–CO_2	−0.106085	0.001127	5.183760e-06	0.000112	0.9999	0.001226
H_2–CH_4	−0.113444	0.001201	5.509623e-06	0.000111	0.9999	0.001306
H_2O–CO	−0.041895	0.000443	2.034715e-06	0.000111	0.9999	0.000482
H_2O–CO_2	−0.034615	0.000361	1.627449e-06	0.000110	0.9999	0.000396
H_2O–CH_4	−0.042982	0.000450	2.045609e-06	0.000110	0.9999	0.000492
CO–CO_2	−0.026500	0.000280	1.281830e-06	0.000111	0.9999	0.000304
CO–CH_4	−0.035039	0.000370	1.696197e-06	0.000111	0.9999	0.000403
CO_2–CH_4	−0.029049	0.000305	1.387365e-06	0.000111	0.9999	0.000332

Constants and operating conditions
R = 8.314; F = 96485; ℓ = 0.00075; cf = 101325; p = 1;
yAin = 0.2; yBin = 0.8; T = 1073;
Binary diffusion: H_2–H_2O system
Fuller method:
MA = 2.016; VA = 6.12;
MB = 18.015; VB =13.10;
VAB = $(VA^{1/3} + VB^{1/3})^2$;
MAB = $2(MA^{-1} + MB^{-1})^{-1}$;
α = 1−**Sqrt**[MA/MB];
ε = 0.30; ξ = 6.0;
DAB = $(\varepsilon/\xi)((0.000143\ T^{1.75})/(p\ MAB^{.5}\ VAB))$;
DAB = DAB/100
Knudsen diffusion:
r = 0.0000005;
DAK = (ε/ξ) (97.0 r **Sqrt**[T/MA])
j = {3000,7500,15000}; ln = **Length**{j};
dusty gas model:

```
Flatten[Table[ {y1 =Evaluate[ y[ℓ] /.
    NDSolve[ {y"[x] + (α/DAB) ((1 − α y[x])/
        DAB + 1/DAK)^−1 y'[x]^2 == 0,
    y[0] = yAin,
    y'[0] = −(j[[m]] R T)/(2 p*cf F) ((1 − α yAin)/(DAB)
        + 1/DAK)^−1},
    y, {x,0,ℓ}]]; y2 =1 − y1;
    − ((R T)/(2 F)) Log[(y1 yBin)/(y2 yAin)]},{m,1,ln}]];
```

References

[1] P. Holtappels, L.G.J. De Haart, U. Stimming, I.C. Vinke, M. Mogensen, Reaction CO/CO_2 gas mixtures on Ni-YSZ cermet electrodes, J. Appl. Electrochem. 29 (1999) 561–568.

[2] E. Achenbach, E. Riensche, Methane/steam reforming kinetics for solid oxide fuel cells, J. Power Sources 52 (1994) 283–288.

[3] P.N. Hutton, M.A. Musich, N. Patel, D.D. Schmidt, R.C. Timpe, Feasibility study of a thermally integrated SOFC-gasification system for biomass power generation, For U.S. Department of Energy National Energy Technology Laboratory Cooperative Agreement. Phase 1. Interim Report, No. DE-FC26–98FT40321, Energy & Environmental Research Center-University of North Dakota, 2003.

[4] S.P. Jiang, Resistance measurement in solid oxide fuel cells, J. Electrochem. Soc. 148 (8) (2001) A887–A897.

[5] K. Sasaki, Y. Hori, R. Kikuchi, K. Eguchi, A. Ueno, H. Takeuchi, M. Aizawa, K. Tsujimoto, H. Tajiri, H. Nishikawa, Y. Uchida, Current–voltage characteristics and impedance analysis of solid oxide fuel cell for mixed H_2 and CO gases, J. Electrochem. Soc. 149 (3) (2002) A227–A233.

[6] P. Costamagna, P. Costa, Vicenzo Antonucci, Micro-modelling of solid oxide fuel cell electrodes, Electrochem. Acta 43 (3–4) (1998) 375–394.

[7] J.W. Kim, A.V. Virkar, K.Z. Fung, K. Mehta, S.C. Singhal, Polarization effects in intermediate temperature, anode-supported solid oxide fuel cells, J. Electrochem. Soc. 146 (1) (1999) 69–78.

[8] S. Sunde, Simulations of composites electrodes in fuel cells, J. Electroceram. 5 (2) (2000) 153–182.

[9] J. Divisek, R. Jung, I.C. Vinke, Structure investigations of SOFC anode cermets. Part II: Electrochemical and mass transport properties, J. Appl. Electrochem. 29 (1999) 165–170.

[10] S.H. Chan, Z.T. Xia, Anode micro model of solid oxide fuel cell, J. Electrochem. Soc. 148 (4) (2001) A388–A394.

[11] S.H. Chan, K.A. Khor, Z.T. Xia, A complete polarization model of a solid oxide fuel cell and its sensitivity to the change of cell component thickness, J. Power Sources 93 (2001) 130–140.

[12] H. Zhu, R.J. Kee, A general mathematical model for analyzing the performance of fuel-cell membrane–electrode assemblies, J. Power Sources 117 (2003) 61–74.

[13] W. Lehnert, J. Meusinger, F. Thom, Modelling of gas transport phenomena in SOFC anodes, J. Power Sources 87 (2000) 57–63.

[14] H. Yakabe, M. Hishinuma, M. Uratani, Y. Matsuzaki, I. Yasuda, Evaluation and modeling of performance of anode-supported solid oxide fuel cell, J. Power Sources 86 (2000) 423–431.

[15] E. Achenbach, Three-dimensional and time-dependent simulation of a planar solid oxide fuel cell stack, J. Power Sources 49 (1994) 333–348.

[16] H. Yakabe, T. Ogiwara, M. Hishinuma, I. Yasuda, 3-D model calculation for planar SOFC, J. Power Sources 102 (2001) 144–154.

[17] M. Iwata, T. Hikosaka, M. Morita, T. Iwanari, K. Ito, K. Onda, Y. Esaki, Y. Sakaki, S. Nagata, Performance analysis of planar-type unit SOFC considering current and temperature distributions, Solid State Ionics 132 (2000) 297–308.

[18] S.H. Chan, Z.T. Xia, Polarization effects in electrolyte/electrode-supported solid oxide fuel cells, J. Appl. Electrochem. 32 (2002) 339–347.

[19] J.M. Smith, H.C. Van Ness, M.M. Abbott, Introduction to Chemical Engineering Thermodynamics, 6th ed., McGraw Hill, 2001.

[20] F.F. Huang, Engineering Thermodynamics, 2nd ed., Macmillan Publishing Company, 1988.

[21] J. Larminie, A. Dicks, Fuel Cell Systems Explained, John Wiley and Sons, Ltd, 2002.

[22] C.G. Motloch, Thermochemical modeling and performance of a methane reforming solid oxide fuel cell, Ph.D. Thesis, Idaho State University, January 1998.

[23] T.M. Maloney, Computer modeling of solid oxide fuel cells, Ph.D. Thesis, Cleveland State University, March 1990.

[24] J.R. Ferguson, Analysis of temperature and current distributions in planar SOFC designs, in: Proceedings of the International Symposium on Solid Oxide Fuel Cells, Comission of the European Communities, July 1991, pp. 305–312.

[25] N.Q. Minh, T. Takahashi, Science and Technology of Ceramic Fuel Cells, Elsevier, 1995.

[26] EG-G Services, Fuel Cell Handbook, 6th ed., Parsons, Inc., Science Applications International Corporation, 2002.

[27] S. Campanari, P. Iora, Definition and sensitivity analysis of a finite volume SOFC model for a tubular cell geometry, J. Power Sources 132 (2004) 113–128.

[28] C. Moler, Numerical Computing with MATLAB, 1st ed., Electronic Edition by Matworks, 2004. www.mathworks.com/moler/

[29] J.W. Veldsink, R.M.J. van Damme, G.F. Versteeg, W.P.M. van Swaaij, The use of the dusty-gas model for the description of mass transport with chemical reaction in porous media, Chem. Eng. J. 57 (1995) 115–125.

[30] R. Suwanwarangkul, E. Croiset, M.W. Fowler, P.L. Douglas, E. Entchev, M.A. Douglas, Performance comparison of fick's, dusty-gas and Stefan–Maxwell models to predict the concentration overpotential of a SOFC anode, J. Power Sources 122 (2003) 9–18.

[31] J.W. Veldsink, G.F. Versteeg, W.P.M. van Swaaij, An experimental study of diffusion and convection of multicomponent gases through catalytic and non-catalytic membranes, J. Membr. Sci. 92 (1994) 275–291.

[32] B. Zhang, X. Liu, Effects of fractal trajectory on gas diffusion in porous media, AIChE J. 49 (12) (2003) 3037–3047.

[33] J. Divisek, R. Wilkenhoner, Y. Volfkovich, Structure investigations of SOFC anode cermets. Part I: Porosity investigations, J. Appl. Electrochem. 29 (1999) 153–163.

[34] J.R. Ferguson, J.M. Fiard, R. Herbin, Three-dimensional numerical simulation for various geometries of solid oxide fuel cells, J. Power Sources 58 (1996) 109–122.
[35] N.F. Bessette, Modeling and simulation for solid oxide fuel cell power systems, Ph.D. Thesis, Georgia Institute of Technology, 1994.
[36] S. Park, J.M. Vohs, R.J. Gorte, Direct oxidation of hydrocarbons in a solid-oxide fuel cell, Nature 404 (March 2000) 265–267.
[37] L. Petruzzi, S. Cocchi, F. Fineschi, A global thermo-electrochemical model for SOFC systems design and engineering, J. Power Sources 118 (2003) 96–107.
[38] R.J. Braun, Optimal design and operation of solid oxide fuel cell systems for small-scale stationary applications, Ph.D. Thesis, University of Wisonsin-Madison, 2002.
[39] T. Horita, K. Yamaji, T. Kato, N. Sakai, H. Yokokawa, Design of metal/oxide interfaces for the direct introduction of hydrocarbons into SOFCs, J. Power Sources 131 (2004) 299–303.
[40] R.C. Reid, J.M. Prausnitz, B.E. Poling, The Properties of Gases and Liquids, 4th ed., McGraw Hill Book Company, 1987.
[41] B. Todd, J.B. Young, Thermodynamic and transport porperties of gases for use in solid oxide fuel cell modeling, J. Power Sources 110 (2002) 186–200.
[42] E. Hernández-Pacheco, M.D. Mann, The rational approximation method in the prediction of thermodynamic properties for SOFCs, J. Power Sources 128 (2004) 25–33.
[43] E. Hernández-Pacheco, Rational approximations, J. Power Sources 128 (2004) 34–44.